Slice imaging of photodissociation of spatially oriented molecules

Lipciuc, ML; van den Brom, A.J.; Dinu, L.; Janssen, M.H.M.

published in
Review of Scientific Instruments
2005

DOI (link to publisher)
10.1063/1.2138691

document version
Publisher's PDF, also known as Version of record

Slice imaging of photodissociation of spatially oriented molecules

M. Laura Lipciuc, Alrik J. van den Brom,[a] Laura Dinu,[a] and Maurice H. M. Janssen[b]
Laser Centre and Department of Chemistry, Vrije Universiteit, de Boelelaan 1083, 1081 HV Amsterdam, The Netherlands

(Received 9 August 2005; accepted 21 October 2005; published online 14 December 2005)

An electrostatic ion lens to spatially orient parent molecules and to image the angular distribution of photofragments is presented. Photodissociation of laboratory-oriented molecules makes it possible to study the dynamics of the dissociation process in more detail compared to photodissociation of nonoriented molecules. Using the velocity map imaging technique in combination with the slice imaging technique, the spatial recoil distribution of the photofragments can be measured with high resolution and without symmetry restrictions. Insertion of orientation electrodes between the repeller and the extractor of a velocity mapping electrostatic lens severely distorts the ion trajectories. The position where the ions are focused by the lens, the focal length, can be very different in the directions parallel and perpendicular to the inserted orientation electrodes. The focal length depends on the exact dimensions and positions of the electrodes of the ion lens. As this dependence is different in both directions, this dependence can be used to correct for the distorted ion trajectories. We discuss the design of an electrostatic ion lens, which is able to orient parent molecules and map the velocity of the photofragments. We report sliced images of photofragments from photolysis of spatially oriented CD_3I molecules to demonstrate the experimental combination of molecular orientation and velocity map slice imaging with good resolution. © *2005 American Institute of Physics.* [DOI: 10.1063/1.2138691]

I. INTRODUCTION

Since the first demonstration by Chandler and Houston[1] in 1987, the application of ion imaging in the field of chemical dynamics has expanded greatly. A decade later a significant improvement in resolution called velocity map imaging was reported by Eppink and Parker.[2] A special ion lens geometry was used to reduce the spatial blurring due to the extended size of the ion source. More recently, Kitsopoulos and co-workers,[3] Suits and co-workers,[4] and Liu and co-workers[5] demonstrated how a slice of the three-dimensional ion cloud can be obtained by spreading the ion cloud in time. This latter method, called slice imaging, has the advantage that there are no restrictions with respect to cylindrical symmetry for analyzing the imaging data. Furthermore, it has been shown that the slice imaging technique appears to provide a better velocity resolution than the conventional velocity map imaging technique.[6,7]

In this article we present the design and operation of an ion lens for slice imaging of fragments from photolysis of laboratory-oriented molecules. Orientation of parent molecules before photolysis can provide additional information on the dynamics of the dissociation of the molecule.[8,9] Orientation of symmetric top parent molecules before dissociation can be accomplished by selecting a single (JKM) rotational state with $M \neq 0$ using a hexapole state selector and retaining the projection M of the total angular momentum J on an external axis by leading the state-selected molecules into a homogeneous electric field. If one of the atoms of the parent molecule has a nonzero nuclear spin I, coupling of I to the rotational angular momentum J will reduce the effective orientation of the molecular axis. The linear electric field must then be relatively high to decouple I and J, in order to keep the molecules fully oriented. For example, an electric field strength of about 1500 V/cm is required to fully decouple the hyperfine interaction and to saturate the degree of orientation in CH_3I molecules in the $(JKM)=(111)$ state.[10]

Photodissociation of oriented CD_3I molecules, followed by imaging of the CD_3 photofragments, was first demonstrated in 1995 using the original ion imaging technique with grids.[11,12] The molecules were oriented in an electric field perpendicular to the extraction field. After switching the electrode voltages in about 20–30 ns (the time interval between the photolysis and ionization laser pulses was set somewhat longer, to about 50–80 ns) from the orientation geometry to the extraction geometry, the ionized photofragments were extracted toward a two-dimensional microchannel plate (MCP)/phosphor-screen detector coupled to a charge-coupled device (CCD) camera. A strong orientation field was accomplished by applying orientation electrodes between the repeller and extractor of a Wiley-McLaren-type electrostatic ion lens.[12] This Wiley-McLaren-type ion lens however has some disadvantages for the application to ion imaging. It is mostly suitable because of its high resolution of mass separation in a time-of-flight (TOF) region, but it suffers from the blurring due to the extended source region of the ions.

The recent developments in velocity map and slice im-

[a]Present address: MAPPER Lithography, Lorentzweg 1, 2628 CJ Delft, The Netherlands.
[b]Author to whom correspondence should be addressed; electronic mail: mhmj@chem.vu.nl

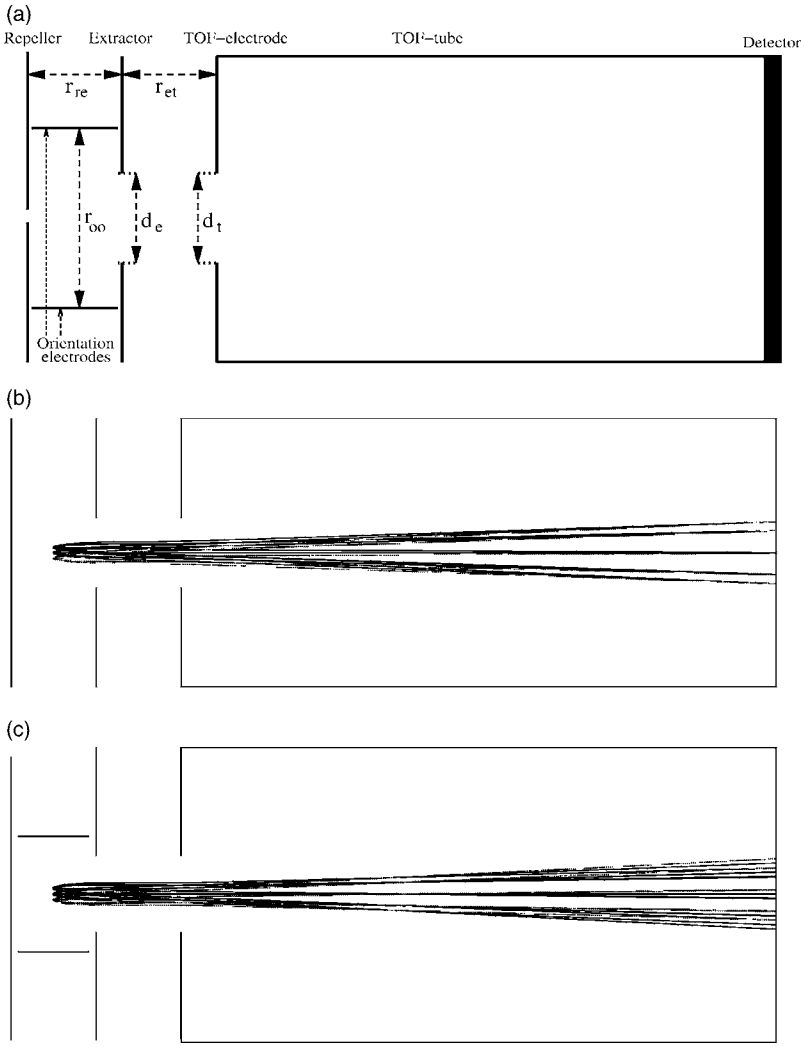

FIG. 1. (a) Definitions of the dimensions describing the electrostatic lens with orientation electrodes. The distance between the repeller and the extractor (r_{re}), the extractor and the TOF electrode (r_{et}), and the two orientation electrodes (r_{oo}) are indicated, as well as the inner diameters of the extractor (d_e) and the TOF electrode (d_t). (b) Demonstration of velocity mapping as described by Eppink and Parker (Ref. 2). The "focal plane" is precisely at the detector plane. Three different initial positions of where the ions are produced are indicated with different gray shades. The applied extractor voltage was 0.7 times the repeller voltage. (c) Distortion of the electric field by the presence of orientation electrodes between the repeller and the extractor during ion extraction. The voltage on the orientation electrodes equals 0.84 times the repeller voltage. The focal plane is shifted towards the electrostatic lens.

aging led us to redesign our ion lens for experiments on spatially oriented photodissociation. In this article we report the design and operation of an ion lens for slice imaging of oriented molecules.

II. DESIGN AND SIMULATIONS

The design principle of the lens was to keep the ion lens as simple as possible and to start from the standard velocity map ion lens, adding the extra electrode plates for orientation. In Fig. 1(a) we show the generic design of the lens. The parameters of the lens are the distance between the repeller and extractor, r_{re}, the distance between the orientation electrodes, r_{oo}, the distance between the extractor and the TOF electrode (which is connected to the TOF tube), r_{et}, the inner diameter of the extractor, d_e, and the inner diameter of the TOF electrode, d_t. For brevity, in the simulations we scale all dimensions relative to r_{re}. Furthermore, the voltages applied to the repeller, the extractor, and the orientation electrodes during ion extraction are referred to as V_{rep}, V_{extr}, and V_{orient}, respectively. The dependence of the "focal length," defined as the distance of the focal plane of the velocity mapping to the ion source, on these parameters is investigated with trajectory simulations using SIMION. For the simulations, three ion sources are used, each in which ions are recoiled in 8 different directions, with 45° interval. The different positions of the ion sources are used to demonstrate the fact that velocity mapping does not depend on this position. The simulations were performed for ions of mass 10 amu, and with an initial kinetic energy of 1 eV. The focal length of the lens depends somewhat on the angle, with respect to the TOF axis, at which the ions are ejected. The focal lengths reported below are those corresponding to the ions ejected at 45°, which is the same as for the ions ejected at 135°, 225°, or 315°.

The starting point for investigating the dependence of the focal length of the ion lens on the positions of (all) the electrodes and the voltages applied to them is the design as introduced by Eppink and Parker.[2] In this default design, $r_{re}=r_{et}=d_e=d_t$, with $V_r > V_e$, as is the case of the electrostatic lens drawn in Fig. 1(b). Just inserting orientation electrodes between the repeller and extractor of a velocity mapping electrostatic lens can severely distort the electric field in the direction of the orientation electrodes. The position where the velocity components of each of the ion sources parallel to the repeller intersect, i.e., the "focal plane," is shifted, as shown in Fig. 1(c). Increasing the distance between the orientation electrodes will diminish this distortion but the effective orientation field strength will be smaller as well. This

makes the electrostatic lens less suitable for orienting parent molecules that require a high field strength for orientation.

In order to obtain velocity mapping in both the directions parallel and perpendicular to the orientation electrodes, the focal lengths, $f_\parallel$ and $f_\perp$, must be the same. The perpendicular focal length $f_\perp$ is strongly affected by the voltage applied to the orientation electrodes. When the spacing between the orientation electrodes r_{oo} is small (≈ 1 or $2r_{re}$), it appears that if $V_{\text{orient}} \leqslant V_{\text{extr}}$, the ion trajectories diverge strongly, and most of the ions will not hit the detector. If $V_{\text{orient}} \geqslant V_{\text{rep}}$, the ion trajectories intersect immediately and form a focal plane before they pass the TOF electrode. In general, $f_\perp$ decreases with increasing V_{orient}, so for any geometry there is a single V_{orient} for which $f_\perp = f_\parallel$. This is shown in Fig. 2(a), from which it can readily be seen that $f_\perp = f_\parallel$ when the solid and corresponding dashed lines intersect.

The inner diameter d_t of the TOF electrode as well as its distance to the extractor can be varied and they both affect the parallel and perpendicular focal lengths. The dependence of $f_\perp$ on the inner diameter d_t is illustrated in Fig. 2(b). The effect of increasing r_{et}, the distance between the extractor and the TOF electrode, shows the same trend, but is stronger. The effect of varying the inner diameter of the extractor, d_e, is similar to the effect of varying d_t, but the effect of moving the extractor forward and backward is opposite to moving the TOF electrode: $f_\parallel$ and $f_\perp$ decrease when r_{re} is increased, and vice versa, whereas $f_\parallel$ and $f_\perp$ increase with increasing r_{et}. In general, the sensitivity of the focal lengths to variations in the extractor geometry (r_{re} and d_e) is larger then variations in the geometry of the TOF electrode (r_{et} and d_t).

The effect of the voltage applied to the extractor, V_{extr}, is shown in Fig. 2(c). As can be seen, the perpendicular focal length $f_\perp$ increases considerably by decreasing the extractor voltage V_{extr}, especially if V_{orient} is low.

III. EXPERIMENTAL RESULTS

As shown in the previous section, a configuration of the ion lens can be chosen in which the focal lengths parallel and perpendicular to the direction of the orientation electrodes are the same. If the magnification factors for both directions differed, squeezing of the ion cloud in one of the directions would cause the detected ion sphere to be "egg-shaped," making the electrostatic lens unsuitable for velocity mapping purposes. A configuration in which no "egg-shaping" occurs was built with the following dimensions: $r_{re}=20$ mm, $r_{et}=35$ mm, $r_{oo}=26$ mm, $d_e=20$ mm, $d_t=30$ mm. The outer diameter of the electrodes is 100 mm. The length of the TOF tube is 400 mm (with respect to the repeller) and the diameter is 40 mm.

The ion lens has to operate in two different modes; one is the ion extraction velocity map imaging mode for which we discussed the optimal configuration in the previous section. The other mode of operation is the orientation mode. In this mode the electrostatic lens has to produce a sufficiently strong and homogeneous electric field to orient the parent molecules before dissociation. The orientation field for the neutral parent molecules is directed perpendicular to the ion extraction field which accelerates the ionized fragments into the time-of-flight tube. The presence of repeller and extractor electrodes on either side of the orientation electrodes influ-

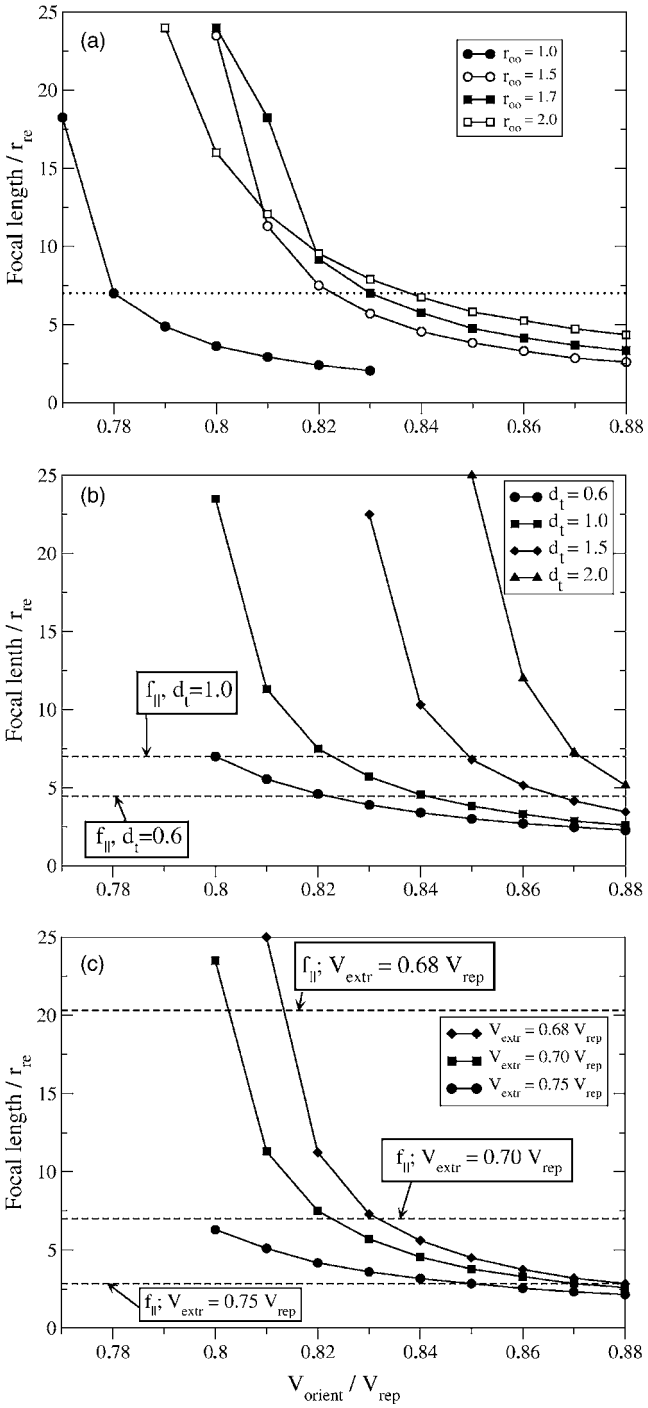

FIG. 2. (a) Dependence of $f_\perp$ on the applied voltage on the orientation electrodes, V_{orient}, for different distances r_{oo} between the orientation electrodes (solid lines). The dashed line is the focal length in the direction parallel to the orientation electrodes, $f_\parallel$. These simulations were done for $V_{\text{extr}}=0.7\ V_{\text{rep}}$. It follows that $f_\perp = f_\parallel$ if the solid and dashed lines intersect. (b) Dependence of $f_\perp$ on V_{orient} for different diameters of the TOF electrode of the electrostatic lens, d_t. The simulations were done with $d_{oo}=1.5$. The dashed lines are the focal lengths in the direction parallel to the orientation electrodes for two different diameters d_t. (c) Dependence of the parallel and perpendicular focal lengths $f_\parallel$ and $f_\perp$ on the voltage applied on the extractor, V_{extr}. The distance between the orientation electrodes, $r_{oo}=1.5$. The dashed lines are the focal lengths in the direction parallel to the orientation electrodes for three different extractor voltages.

ences the effective orientation field strength in the laser interaction region. A way to enhance the effective orientation field is splitting the repeller and extractor electrodes into an upper and a lower half. If a positive voltage is applied to the upper repeller, orientation and extractor electrodes, and a negative voltage to their lower counterparts, a higher electric field is obtained than when only a voltage difference is applied to the orientation electrodes themselves. By splitting the repeller and extractor electrodes the distance between the orientation electrodes can be enlarged and a high orientation field strength still can be obtained. The electric field strength in the center of the electrostatic lens (i.e., 10 mm to the right of the repeller) is sensitive to both the voltage differences between the extractor halves and between the repeller halves. It is favorable to keep the electric field homogeneous, in order to be less sensitive to the position where the photolysis laser intersects the (oriented) molecular beam. By selecting the voltages applied to the upper and lower repeller and extractor, a homogeneous electric field in the region in the middle between the repeller and the extractor is obtained. Great care was taken to make both parts of the repeller and extractor electrodes parallel, which is important to avoid a possible deformation in the image.

To demonstrate the performance of the electrostatic lens we performed a photodissociation experiment on CD_3I molecules state selected in the $(JKM)=(111)$ state using a hexapole.[12,13] Voltages of 3 kV on the upper orientation electrode and −3 kV on the lower orientation electrode were applied to orient the parent molecules before they were photolyzed by a pulsed laser at 266 nm. Approximately 10 ns after the photolysis laser, the orientation field was switched to an extraction field using $V_{rep}=1305$ V, $V_{orient}=1115$ V, and $V_{extr}=1008$ V. After ~50 ns, the CD_3 photofragments were ionized by a second laser at 333.75 nm. The time delay between pump and probe was set to give sufficient time to have some initial ringing in the voltages that are switched to be damped. But, as discussed below, this ringing appeared to have no significant negative effect on the slicing as the resolution obtained for the oriented and nonoriented experiment appears to be very similar. The ionization was done via the Q branch of the 0_0^0 band, using a (2+1) resonantly enhanced multiphoton ionization (REMPI) scheme via the $3p_z$ intermediate Rydberg state. This transition is not sensitive to the alignment of the CD_3 photofragment. The polarization of the photolysis laser was parallel to the plane of the detector; the polarization of the probe laser was perpendicular to the plane of the detector. The timing sequence for the experiment on the nonoriented and oriented parent molecules is shown in Fig. 3. For the nonoriented molecules the voltages on the electrodes were also pulsed to have similar electric field conditions and ringing from switching fields as in the case of the oriented molecules. Only the timing of the laser pulses was set differently for the two experiments. For the nonoriented case the timing was such that the two laser pulses came after switching the fields to the extraction geometry, sequence (1) in Fig. 3. For the oriented case the timing was set such that the pump laser pulse came before the switching of the electric fields and the probe pulse after the switching, sequence (2) in Fig. 3. The overshoot and ringing of the voltages on

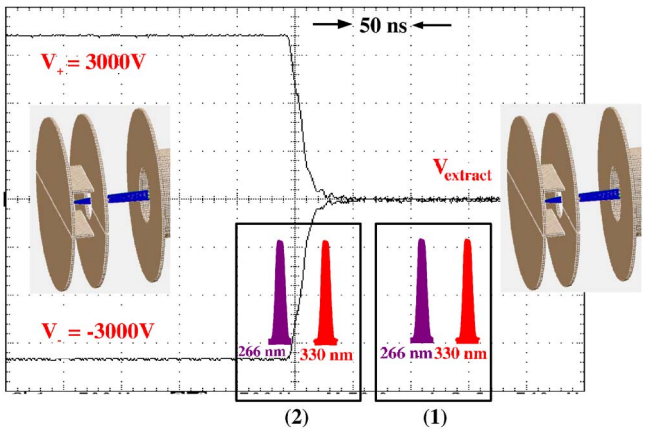

FIG. 3. (Color online) Timing sequence of the experiment. The voltages on the electrodes are switched with high-voltage switches (Behlke Electronic GmbH) from the orientation field geometry to the extraction field geometry. In the orientation field geometry the typical voltages used on the upper and lower orientation electrodes are 3000 and −3000 V, respectively. To measure the photofragment image for photodissociation of a nonoriented parent molecule the pump and probe pulses are fired after the voltages are switched to the extraction geometry, sequence (1). To measure the image for photodissociation of an oriented parent molecule, e.g., in the $(JKM)=(111)$ state, the pump and probe lasers are triggered earlier, such that the switching of the voltages on the electrodes is between the pump and probe laser pulses, sequence (2). Note that in both cases the high voltages on the electrodes is switching so in both cases ringing of the voltages on the electrodes for the extraction geometry is present.

the electrodes was minimized by adding small resistors (typically less than 100 Ω) in series with all the electrodes. The extra resistor slows down the fast rising part of the high voltage pulse somewhat but significantly reduces the overshoot of the pulse.

Although we pulse voltages on the ion electrodes we do have a constant and nonzero electric field in the extraction region when we ionize the neutral fragments. As such, we are not doing the pulsed field slice imaging variant as developed by Kitsopoulos and co-workers[3] but the dc slice imaging variant developed by Suits and co-workers,[4] however, with no extra lenses but using the standard velocity map lens geometry. The extraction fields are relatively strong, about 140 V/cm; to obtain still a relatively narrow slice we need a fast high-voltage (HV) pulse on the MCP detector. For the slicing of the fragment cloud we pulse the gain of the MCP detector with a home-built fast HV pulser. The light of the phosphor screen is imaged on a 2048 by 2048 pixels CCD camera. To demonstrate that real slices are made, we show in Fig. 4 a sequence of 11 images for photodissociation of nonoriented parent molecules. Each image was taken with 2 min of total exposure time (about 1200 laser shots per image), and the HV pulser is set at a certain delay with respect to the laser pulse, indicated by the time in the corner of the individual images. Clear slices through the ion cloud are made by the HV pulser, and the total observed time-of-flight arrival time spread is about 80–90 ns. The images further away from the center are smaller in radius and show a larger spread in the radial recoil distribution as expected for a parallel transition; see also the discussion below. As the recoil distribution reflects a parallel distribution, very low intensity is measured for the fragments recoiling away and towards

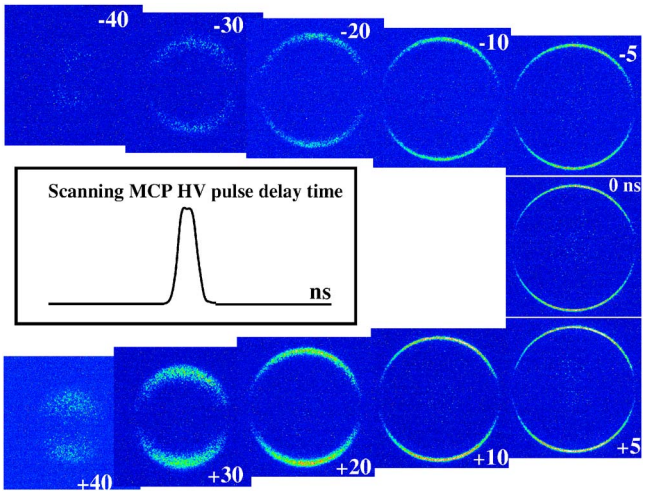

FIG. 4. (Color online) Raw data images as observed for detection of the CD_3 0_0^0 photofragment after photolysis at 266 nm of nonoriented parent molecules. The HV pulse was scanned over the total time-of-flight arrival time spread of about 80–90 ns. Each image was 2 min of total measuring time.

the detector plane, i.e., those fragments that will show up at the far wings of the time-of-flight distribution, about −40 ns and 40 ns on either side of the center of the total TOF spread. We will further discuss the effective slice width of the HV pulser below.

In Fig. 5 we present the experimental images of the sliced photofragment recoil for both nonoriented and oriented parent molecules at the middle of the time-of-flight arrival spread. The voltages applied on the orientation electrode were such that the methyl side of the parent molecule was oriented upward in the laboratory frame. For the nonoriented photodissociation, the image in Fig. 5(a) shows the well-known rings in the upper and lower half with near-$\cos^2\theta$ intensity distribution, with θ the angle between the vertical direction of the polarization of the pump laser and the recoil direction of the fragment. For the oriented photodissociation it can be seen from Figs. 5(b) and 5(c) that the parent molecules are spatially fully oriented along the vertical direction (see also below). Only a few photofragments are recoiling in the direction of the lower part of the image. This can be better observed in Fig. 5(c), where we have clipped the intensity scale to show the low intensity in the lower half of the image.

The angular distributions from the sliced images are shown in Fig. 6. Also, the theoretically calculated angular distributions of the nonoriented and the oriented (111) state are plotted. The 266 nm excitation of CD_3I occurs almost exclusively to the $^3Q_0$ state which is accessed through a parallel transition.[14] We ionize the CD_3 via the Q branch of the $3p_z$ intermediate state, and this detection scheme is not sensitive to the alignment of the CD_3 fragment. From the nonoriented image we fit an anisotropy parameter $\beta=1.82$. We used this same value of β to calculate the angular distribution of photofragments from oriented parent molecules in $(JKM)=(111)$ and a fast axial recoil using the probability density functions as given by Choi and Bernstein.[15] As can be clearly seen in Fig. 6, the initial molecular orientation of

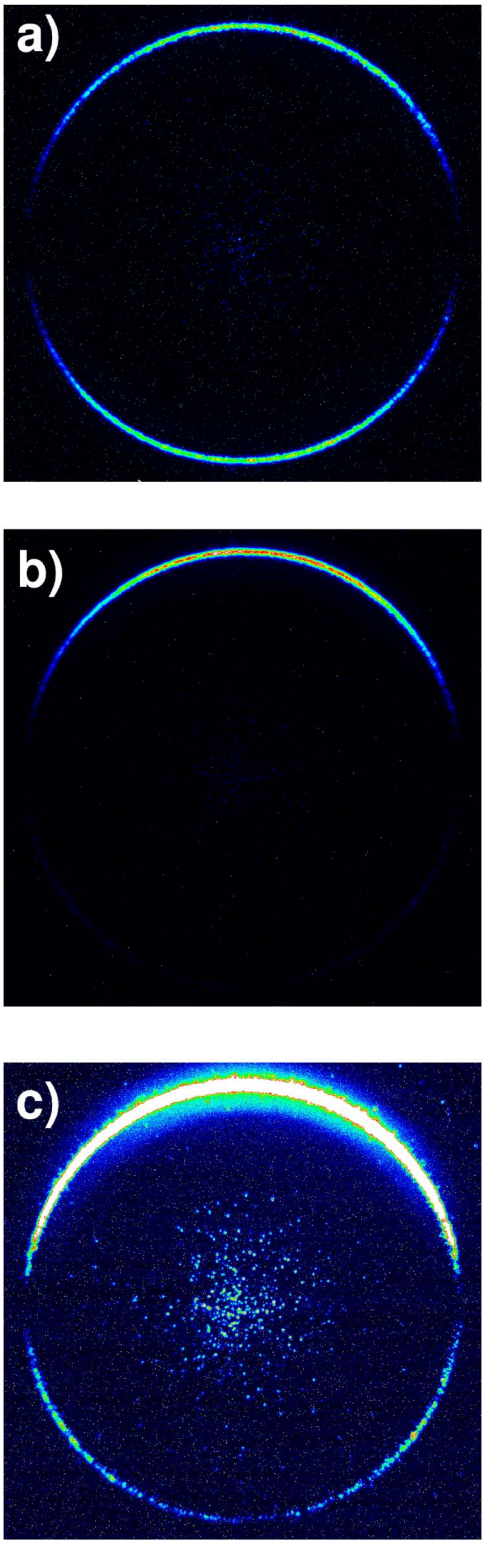

FIG. 5. (Color online) Raw data images as observed for detection of the CD_3 0_0^0 photofragment after photolysis at 266 nm of CD_3I. (a) Nonoriented parent molecule. (b) $(JKM)=(111)$-oriented parent molecule with full-scale intensity range. (c) $(JKM)=(111)$-oriented parent molecule, but the scale of image (b) was clipped to 6% of the maximum to show the small intensity in the lower half of the ring. For all images, the total image size is 1800 by 1800 pixels on the CCD and the exposure time was 5 min, corresponding to about 3000 laser shots.

the CD_3I parent molecule is reflected in the angular distribution of the CD_3 photofragments. The experimental results are in good agreement with the theoretical angular distributions.

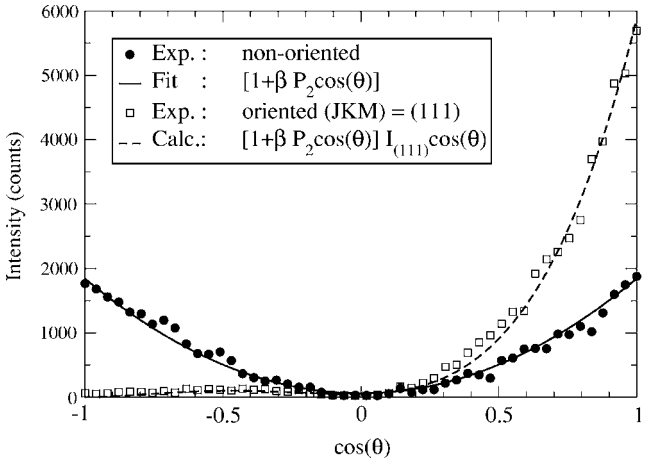

FIG. 6. Angular distributions of the CD_3 0_0^0 photofragments after photolysis of nonoriented and oriented CD_3I at 266 nm. The distributions were obtained from Figs. 5(a) and 5(b). The solid dots are the experimental data points for the nonoriented CD_3I, the squares for the oriented CD_3I. The solid line through the nonoriented data points is the best fit with $\beta=1.82$. The solid line through the oriented data points is a calculated theoretical distribution with the same β parameter and the theoretical orientation distribution for a fully oriented $(JKM)=(111)$ state (Ref. 15). Note that the measured intensity ratio at $\cos(\theta)=1$, $I_{(JKM)=(111)}/I_{\text{nonoriented}}\approx 3.2$, in very good agreement with the theoretically expected value of $(2J+1)=3$.

When the delay of the HV pulse on the MCP detector is set such that the slice goes through the middle of the ion cloud distribution, as was done for the images in Fig. 5, the sliced image provides the velocity distribution directly. The radial velocity distribution of the CD_3 photofragments from the oriented molecules is shown in Fig. 7. We integrated the radial distribution along the total $(0-2\pi)$ angular range of the sliced image. As can be seen in Fig. 7, the velocity distribution is quite narrow, with a relative resolution of $\Delta v/v=2.6\%$. This indicates that the CD_3 photofragments are well sliced and mapped on the detector. The distribution for the nonoriented image is very similar, with a relative resolution of $\Delta v/v=2.7\%$. This shows that the somewhat larger amplitude of the ringing of the voltages on the electrodes [see sequence (2) in Fig. 3] has no influence on additional blurring of the image.

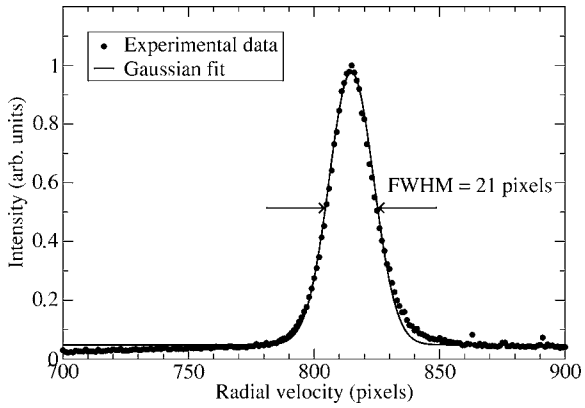

FIG. 7. Radial velocity distribution (in pixels of CCD) of the CD_3 photofragments after photolysis of oriented CD_3I $(JKM)=(111)$ at 266 nm. The radial distribution was obtained from a full angular integration of Fig. 5(b). The solid curve is a Gaussian fit with a full width at half maximum (FWHM) of 21 pixels. This means that the relative velocity resolution $\Delta v/v=2.6\%$.

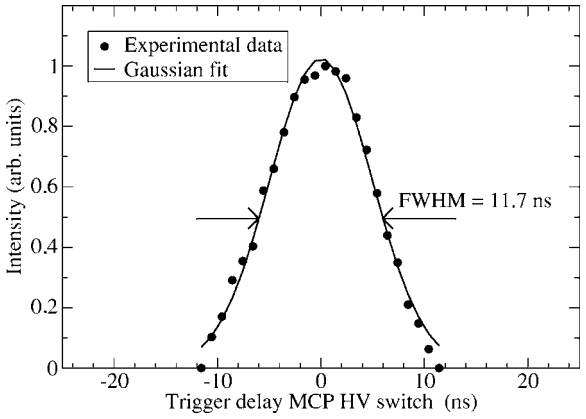

FIG. 8. Effective gain width of the MCP detector using the fast HV pulser. The measured intensity (solid dots) of the CD_3I parent ion yield on the detector is plotted as a function of the time delay of the trigger to the HV switch. The constant bias voltage of the applied voltage on the MCP was 300 V and the amplitude of the narrow HV pulse was 900 V, resulting in a total gain voltage applied over the chevron MCP of 1200 V. The solid line is a Gaussian fit with a FWHM=11.7 ns. This is the effective slice width of our detection system.

To investigate the origin of the radial velocity resolution we measured the effective gain width of our fast HV pulser of the MCP detector. This was measured on the CD_3I parent ion molecule, which has a vanishing forward-backward arrival time spread. In Fig. 8 we show the ion intensity when we scan the HV time delay over the TOF of the CD_3I parent ion molecule. As can be seen,we have an effective gain width of about 12 ns, which is about 60% of the shortest electrical pulse our HV pulser can generate. Because the MCP plates have a very nonlinear gain, we can set the bias voltage on the plates relatively low so that the effective width of the MCP is only determined by the upper part of the applied HV pulse. This improves and narrows the effective slice width to about 12–15 ns depending on the level of the bias voltage. Ion trajectory simulations indicate that the forward-backward time spread at these ion extraction voltages is about 90 ns, in good agreement with our timed slices shown in Fig. 4. This means we slice a part of about 13% of our three-dimensional cloud. The simulations also indicate that the effective slice is at present the limit in the velocity resolution. In many cases this resolution of about 2%–3% is however more than sufficient for experiments with oriented molecules. The width of the slice that can be obtained is influenced by the recoil speed, as this will effect the final arrival time spread. In the results presented here we have a typical kinetic energy of the recoiling fragments of 1.14 eV. We set the voltages such that these fragments reach the outer rim of the detector. Fragments with much lower recoil speed will have a shorter arrival time spread; still, for fragments with a recoil energy of 0.2 eV the arrival time spread is about 40 ns using the same ion lens voltages. This means that for these much slower fragments a slice of about 30% is still obtained with the 12 ns gate. Of course, one can set the ion lens voltages much lower so that they reach the outer edges of the detector. This increases the arrival time spread for low-speed fragments and again one can obtain a slice of about 10%–15%.

Nevertheless, we are currently improving our effective slice by incorporating an additional electrode to lower the

extraction field in the region between the repeller and extractor for dc slicing as proposed by Suits and co-workers.[4] With the extra electrode we will be able to stretch the arrival time spread of the ion cloud to about 200–300 ns. Furthermore, a faster HV pulser with a shorter pulse width will also improve the effective slice and narrow the velocity resolution. We will report on such experiments in the future.

IV. DISCUSSION

The focal length of a velocity mapping electrostatic lens, in which orientation electrodes are inserted between the repeller and extractor, depends on the geometry of its electrodes and the applied voltages. This dependence is different in the direction of the orientation electrodes and allows compensation for the distortion of the electric field, which is introduced by the presence of the orientation electrodes. This difference is used to design an electrostatic lens which allows orientation of parent molecules and, after switching the voltages from orientation to extraction settings, allows velocity mapping of the ionized photofragments. The field strength for the molecular orientation can be made efficient and sufficiently homogeneous in the middle between the repeller and extractor by splitting these electrodes into an upper and a lower part. It is shown experimentally that it is possible to velocity slice and map the recoil of the photofragments from oriented parent molecules with switching high voltages on the ion lens electrodes. A radial velocity resolution of $\Delta v/v = 2.6\%$ is obtained, enabling quantitative measurement of slice images with sufficient resolution. The ion lens provides slice imaging of fragments from oriented photodissociation with good quantitative accuracy.

ACKNOWLEDGMENTS

This research has been financially supported by the Councils for Chemical Sciences and Physical Sciences of the Dutch Organization for Scientific Research (NWO-CW, NWO-FOM). The authors would like to thank Han Voet for the design of the fast HV MCP pulser, Lex van der Gracht for the design of the fast ion optics voltage switcher, Rob Kortekaas for building the ion lens, and Joost Buijs for his design of the software to read out the large-size CCD camera.

[1] D. W. Chandler and P. L. Houston, J. Chem. Phys. **87**, 1445 (1987).
[2] A. T. J. B. Eppink and D. H. Parker, Rev. Sci. Instrum. **68**, 3477 (1997).
[3] C. R. Gebhardt, T. P. Rakitzis, P. C. Samartzis, V. Ladopoulos, and T. N. Kitsopoulos, Rev. Sci. Instrum. **72**, 3848 (2001).
[4] D. Townsend, M. Minitti, and A. G. Suits, Rev. Sci. Instrum. **74**, 2530 (2003).
[5] J. J. Lin, J. Zhou, W. Shiu, and K. Liu, Rev. Sci. Instrum. **74**, 2495 (2003).
[6] D. Chestakov, S.-M. Wu, G. Wu, D. Parker, A. Eppink, and T. Kitsopoulos, J. Phys. Chem. A **108**, 8100 (2004).
[7] W. Li, S. Chambreau, S. Lahankar, and A. Suits, Rev. Sci. Instrum. **76**, 63106 (2005).
[8] C. A. Taatjes, M. H. M. Janssen, and S. Stolte, Chem. Phys. Lett. **203**, 363 (1993).
[9] T. P. Rakitzis, A. J. van den Brom, and M. H. M. Janssen, Science **303**, 1852 (2004).
[10] J. Bulthuis, J. B. Milan, M. H. M. Janssen, and S. Stolte, J. Chem. Phys. **94**, 7182 (1991).
[11] J. W. G. Mastenbroek, C. A. Taatjes, K. Nauta, M. H. M. Janssen, and S. Stolte, J. Phys. Chem. **99**, 4360 (1995).
[12] M. H. M. Janssen, J. W. G. Mastenbroek, and S. Stolte, J. Phys. Chem. A **101**, 7605 (1997).
[13] A. J. van den Brom, T. P. Rakitzis, J. van Heyst, T. N. Kitsopoulos, S. R. Jezowski, and M. H. M. Janssen, J. Chem. Phys. **117**, 4255 (2002).
[14] A. T. J. B. Eppink and D. H. Parker, J. Chem. Phys. **109**, 4758 (1998).
[15] S. E. Choi and R. B. Bernstein, J. Chem. Phys. **85**, 150 (1986).